Surface & Coatings Technology 305 (2016) 76–82

Contents lists available at ScienceDirect

Surface & Coatings Technology

journal homepage: www.elsevier.com/locate/surfcoat

Heredity and variation of hollow structure from powders to coatings through atmospheric plasma spraying

Pei-Hu Gao [a,b], Guan-Jun Yang [b,*], Si-Ting Cao [a], Jian-Ping Li [a], Zhong Yang [a], Yong-Chun Guo [a]

[a] School of Materials and Chemical Engineering, Xi'an Technological University, Xi'an, Shaanxi 710021, China
[b] State Key Laboratory for Mechanical Behavior of Materials, Xi'an Jiaotong University, Xi'an, Shaanxi 710049, China

ARTICLE INFO

Article history:
Received 29 March 2016
Revised 15 July 2016
Accepted in revised form 3 August 2016
Available online 4 August 2016

Keywords:
Pore
Hollow structure
3D structure
Coating
Atmospheric plasma spraying

ABSTRACT

The pore structure is of significance to both thermal barrier performance and compliance of plasma-sprayed thermal barrier coatings (TBCs). In order to tune the pore structure of plasma-sprayed TBCs, the heredity and variation of the hollow structure from hollow spherical powders (HOSP) to coatings were investigated. Different plasma arc powers were selected for spraying the ceramic coatings. The recollected powders sprayed into water were examined to reveal the microstructure of the powders after arc heating. The results showed that the HOSP structure of spray powder could be retained after heating in plasma arc. Therefore, these hollow structures could be retained into the coating. As a result, four types of pores were formed in the coating. The porosities of the coatings were decreased with the increase in the arc power. Therefore, low arc powers were more suitable to retain the HOSP structure into the coating.

© 2016 Elsevier B.V. All rights reserved.

1. Introduction

Yttria stabilized zirconia (YSZ) is often used for thermal barrier coatings (TBCs) which are widely used in gas turbine engines for the aeronautical and energy production industries [1–6]. The thermal barrier performance of TBCs is dominantly determined by the thermal conductivity in the out-plane direction of the coating [7–10]. A low thermal conductivity and high thermal barrier effect could ensure a superior engine performance mainly by improving the combustion efficiency [3–9]. The thermal conductivity of the coating depends on both the intrinsic thermal conductivity of the bulk material and the porous architecture of the coating [8–13]. Kulkarni et al. [14,15] and Bertrand et al. [16] investigated the effect of feedstock powder structure on the thermal conductivity of the coating. Results show that the thermal conductivities of coatings sprayed from fused and crushed powder (FCP), agglomerated and sintered powder (ASP) and hollow spherical powder (HOSP) were 0.95 ± 0.02, 0.89 ± 0.02, and 0.64 ± 0.01 $W \cdot m^{-1} \cdot K^{-1}$, respectively. [14–17] Clearly, a hollow spherical structure of the HOSP could bring a lower thermal conductivity.

Recently, Wang et al. [15] found that the coatings prepared with HOSP powder showed a larger density of the intersplat pores than those prepared by other feedstock materials including agglomerated/sintered powder (ASP), fused or sintered and crushed powders (FCP), sol-gel powders. Consequently, the resultant YSZ coating's thermal conductivity was significantly reduced [15,18]. Meanwhile, Ercan et al. [19] noticed that, despite the coatings made from HOSP having a higher porosity than the coatings made from ASP, both coatings had the same thermal conductivity. Kulkarni et al. [14,15] found that the minimum thickness of the splats formed by HOSP resulted in a large number of intersplat pores which led to a reduction of the thermal conductivity. Apparently, the evolution of the hollow spherical structure from feedstock powders to the coatings and the pore characters were not clarified clearly which might be related closely to the coating's thermal conductivity.

In the present work, APS 8YSZ coatings were prepared on Ni-base alloy surface using HOSP feedstock powder. The effect of plasma arc power on the evolution of the hollow spherical structure from the powders to the coatings was investigated with an aim at retaining the hollow structure into the coating towards a further ultralow thermal conductivity.

2. Experimental material and procedure

2.1. Materials and coating deposition

The feedstock was a commercially available 8YSZ powder (Sulzer Metco 204NS, d_{10} = 16 μm, d_{50} = 57 μm, d_{90} = 95 μm) with a hollow

* Corresponding author.
E-mail address: ygj@mail.xjtu.edu.cn (G.-J. Yang).

http://dx.doi.org/10.1016/j.surfcoat.2016.08.007
0257-8972/© 2016 Elsevier B.V. All rights reserved.

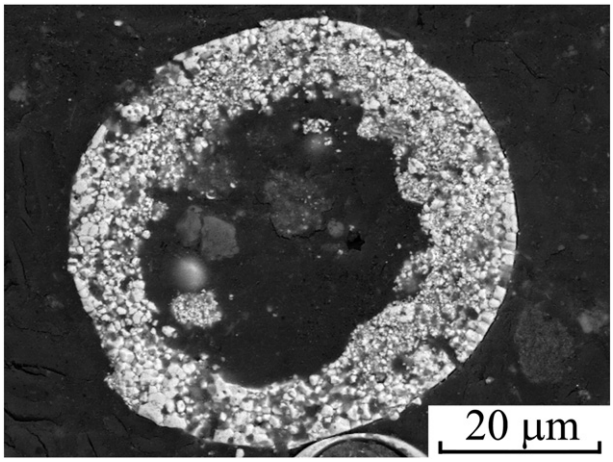

Fig. 1. Cross section of the original feedstock powders.

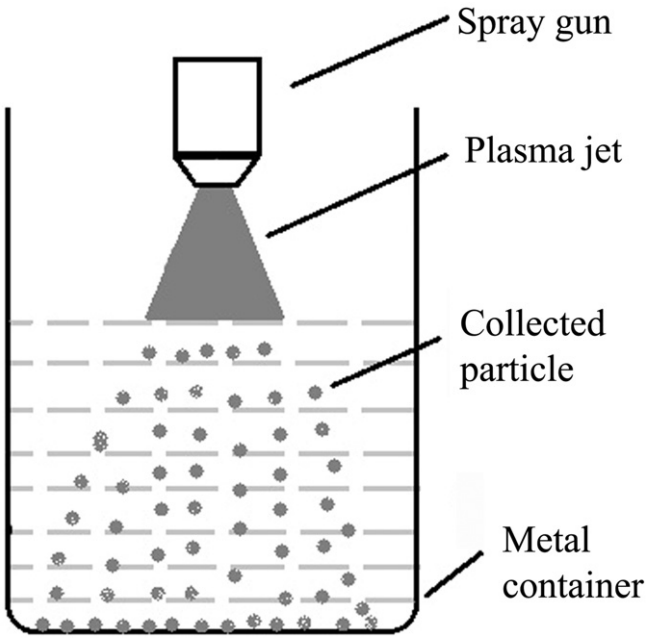

Fig. 2. Sketch of the powder collection set-up.

spherical morphology as shown in Fig. 1. The powder shell was agglomerated of the YSZ particles. There were small pores existed in the powder shells.

The coating deposition was carried out with the spray gun traverse speed of 300 mm/s. A commercial plasma spray system ZB-80 (Zhenbang, China) of 80 kW power was used. The plasma spray parameters were listed in Table 1. Argon was used as a primary plasma operating gas and hydrogen was used as an auxiliary gas. During spraying, the pressures of both argon and hydrogen were fixed at 0.9 and 0.3 MPa, respectively. Three arc powers of 35 kW, 40 kW and 45 kW were applied. To tune the arc power, the hydrogen auxiliary gas flow varied from 4.7 l/min to 6.7 l/min. Argon was used as powder feed gas, and the powder feed rate was about 8 g/min. The spray distance was kept at 80 mm.

2.2. Collection of sprayed powders

In order to identify whether the hollow spherical structure of the feedstocks could be inherited into to the coatings, powders after being heated in plasma arc were recollected and analyzed. The powder was sprayed into distilled water after heating in plasma arc with the plasma torch fixed stationary to the vessel center, as sketched in Fig. 2. The stainless steel vessel with a size of Φ700 × 1200 mm contained 2/3 volumes of distilled water for preventing water splashing outside of the vessel when the heat of plasma plume arrived.

2.3. Microstructure characterization

The feedstock powder, the collected powder in distilled water and the coating were observed by scanning electron microscopy (SEM, Tescan Vega, Czech). The porous structure of the coatings was characterized by X-ray tomography (XRT). An Xradia Versa XRM-500 (Carl Zeiss Microscopy GmbH, Germany) desktop system was applied with the acceleration voltage of 140 kV. The sample was placed between the X-ray source and a 2048 × 2048 pixel array CCD detector equipped with a lens of 10×. The exposure time was 8 s for each of 984 projections while the sample was rotated 360° along its vertical axis. The projection data was reconstructed by a filtered back projection algorithm, and then processed and visualized with the software Avizo Fire®. Both the geometrical magnification and the optical magnification resulted in a voxel size of 1.1299 μm. Pores smaller than one micron was characterized by nitrogen adsorption-desorption method (TriStar II, Micromeritics, USA). The pore size distribution was obtained by using Barrett-Joyner-Halenda method for the isotherms.

3. Results and discussion

3.1. Structure evolution of individual powder after heating in plasma arc

The plasma arc power affects the melting degree of the feedstock powder. Fig. 3 shows the cross section of the collected powder in distilled water with different plasma arc powers. The feedstock was semi-molten under all three plasma power conditions. With the

Table 1
Plasma spray parameters.

Power /kW	Voltage /V	Current /A	Primary gas (Ar)		Auxiliary gas (H_2)	
			Pressure/MPa	Flow/L/min	Pressure/MPa	Flow/L/min
35	63.7	550	0.9	43.4	0.3	4.7
40	66.7	600	0.9	46.3	0.3	5.6
45	70.3	640	0.9	57.6	0.3	6.7

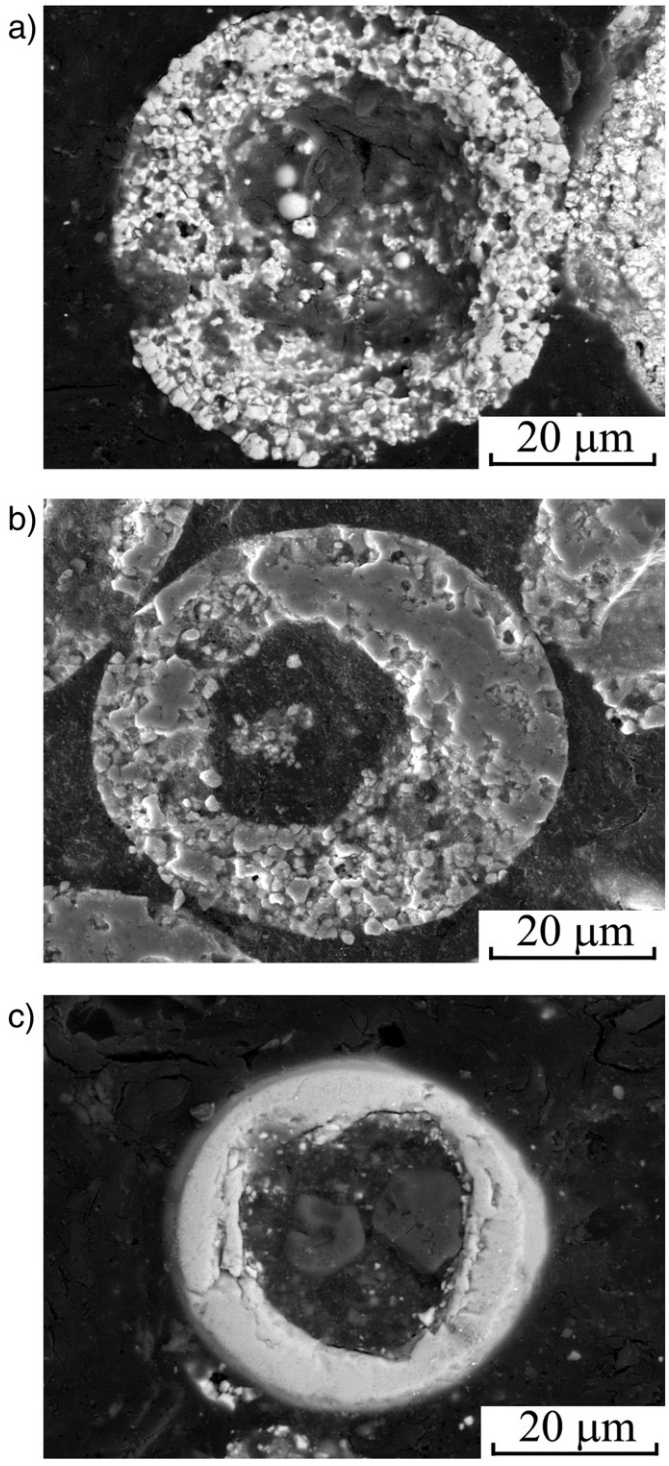

Fig. 3. Cross sections of the collected powders in distilled water with the arc power of (a) 35 kW, (b) 40 kW and (c) 45 kW.

increase of plasma arc power to 45 kW, the shell's porous structure was molten gradually and the powder shell became dense. The hollow spherical structure was still kept in the collected powders after being heated in the plasma arc.

3.2. Coating deposition

Fig. 4 shows the cross sections of the coatings deposited under the arc powers of 35 kW, 40 kW and 45 kW. It was found that there were large and small pores in the coatings deposited with all three plasma arc powers. The pores were in microns (marked as arrows B and C in Fig. 4) to over twenty microns (marked as arrows A in Fig. 4). Some pores were connected each other (seen as arrows C in Fig. 4), some pores were individual (seen as arrows A and B in Fig. 4). Connected pores were similar to the segmentation cracks which were reported in the work of Guo et al. [20]. Finally, extremely small pores, as shown by arrows D, can also be found in Fig. 4.

Meanwhile, all coatings showed a laminar structure, and the intersplat interfaces might be a barrier for heat transfer along the direction perpendicular to the coating surface. These interfaces would inevitably result in a low thermal conductivity. Wang et al. [18] found that the coatings prepared with HOSP showed a larger density of the intersplat interfaces than that prepared by ASP, FCP, sol-gel powders. Consequently, the resultant YSZ coating's thermal conductivity was significantly reduced. Furthermore, there were partly unconnected interfaces which could be the closed regions as similar to the closed pores as marked by arrows B in Fig. 4. Therefore, they were also helpful to reduce the thermal conductivity of the coating. Some small pores among the unmolten 8YSZ particles, particularly in the unmolten shells, were directly inherited from the feedstock hollow structure as marked by arrows D in Fig. 4.

3.3. Pore structure of the coating

Fig. 5 shows the three dimensional (3D) distributions of the pores in the coatings characterized by XRT technology. The pores in the coatings presented an irregular morphology. To quantitatively measure the pore size and porosity, the pores were supposed to be spherical so that the equivalent diameters could be deduced following the methods reported in literature [21,22]. The different colors represented different equivalent diameters of the pores.

Since the pore volume was in cubic power to the pore diameter, the pore volume distribution was also estimated. The pore volume fraction and cumulative volume fraction corresponding to the pore equivalent diameter were both shown in Fig. 6. The pore cumulative volume fraction of the coatings deposited under the arc power of 35 kW, 40 kW and 45 kW were shown in Table 2. With the increase of plasma arc powers from 35 kW to 45 kW, the coating porosity was decreased from 15.9% to 4.2%.

The pore larger than one micron was characterized clearly by the XRT technology. Meanwhile, there also existed some pores smaller than one micrometer. Therefore, it is necessary to examine the volume and distribution of the small pores, which may take effects to the heat transfer and thermal shock resistance. Nitrogen adsorption-desorption analysis was used to characterize the small pore distributions. Figs. 7 and 8 shows the small pore distribution of original powder, recollected powders after being heated in plasma arc and the coatings deposited with the arc power of 35 kW, 40 kW and 45 kW. All small pores were smaller than 125 nm. Meanwhile, there were parts of pores smaller than 20 nm existed in the original powders, which disappeared after the coating deposition. In the coatings, the pore size concentrated in 20 to 65 nm. Quantitative calculation yielded that the total porosities of the nano-sized pores in the coatings are less than 1%. Therefore, the total porosity is evidently determined by the large pores as shown in Fig. 6. In addition, the density of the coatings were also tested and listed in Table 2. The densities were consistent with the porosities of the three types of coatings.

3.4. Formation of pores in the coating

The examination of the recollected powders into water after plasma arc heating shows that the feedstock powders were partially melted in the shell parts after being heated in the plasma jet with the power of 35 kW, 40 kW and 45 kW. The hollow spherical structures were mainly

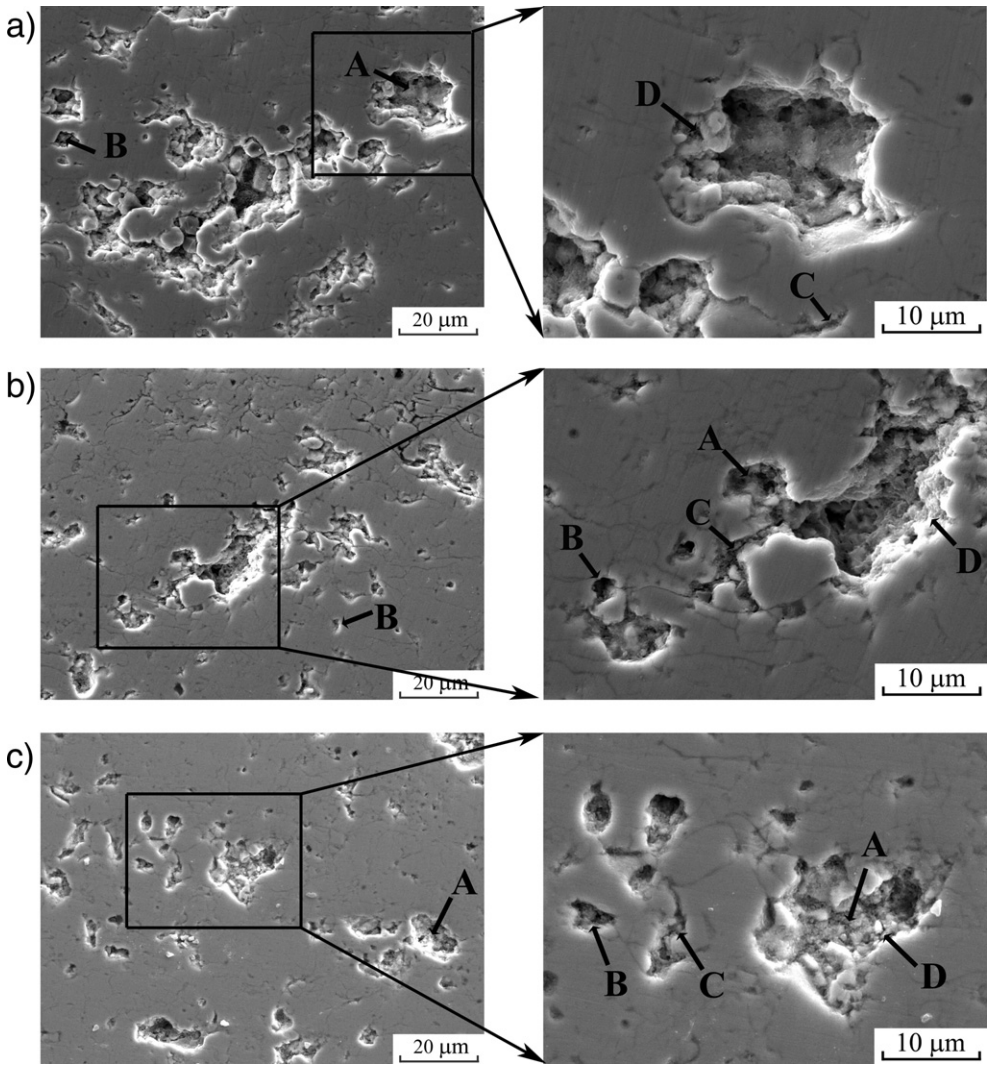

Fig. 4. Cross sections of the coatings deposited with different arc powders: (a) 35 kW, (b) 40 kW and (c) 45 kW. A refers to the large pores inherited from the HOSP structure of the feedstock, B refers to the connected pores between individual splats, C refers to the intra-splat cracks, and D refers to the nano-pores from the feedstock.

inherited after heating the powder in plasma jet. After impacting onto the substrate surface, they deformed intensively. The deposition processing of the hollow spherical powder was simulated by Arvind Kumar [23]. When the HOSP powders impacted onto the substrate surface, the core hollow structure would be broken into several new small hollow pores.

With the increase of plasma arc power, the melting degree of the powders was increased. As shown in Fig. 3, the shell parts of the collected powders became denser in the plasma arc of 45 kW than those in 35 kW and 40 kW. Therefore, in the deposition processing, the deformation degree of the powder was increased with the plasma arc increasing [24,25] so that both of the core hollow structure and shell pores would be drove away more easily in 45 kW than in 35 kW and 40 kW. From the heating to the impacting of the hollow spherical powders onto the bond coat surface, there were some pores inherited from the powders with hollow spherical structure as well as some pores newly formed from the broken parts of the middle parts of the hollow structure.

As comparison of the pore size distribution between the original powders and recollected powders after heating in the plasma arc, the volume of the pores smaller than 20 nm decreased obviously after heating in plasma arc. Meanwhile, with the plasma arc power increased to 45 kW, the volume of the pores smaller than 120 nm decreased a little. It was confirmed that nanostructured pores were mainly retained and not destroyed during heating in the plasma arc, which might be retained into coatings.

From the cross sections of the YSZ coatings deposited with 8YSZ HOSP powders with the plasma spray arc powers of 35 kW, 40 kW and 45 kW, there were some spherical or elliptical closed pores which were mainly inherited from powders' hollow spherical structure as marked by arrows A in Fig. 4. The pores larger than one micron were characterized clearly through XRT as shown in Fig. 5 and counted statistically as shown in Fig. 6. From the 3D view, some pores were individual and some pores connected each other in three direction. The three directional size of the pores matched the cross sectional pore size very well. Meanwhile, there were some open pores mainly existed in the shells of the feedstock powders as marked by arrows D in Fig. 4. The geometries of these open pores were small and could be characterized through nitrogen absorption desorption analysis as shown in Fig. 8. The small pores with nano-size were inherited from the original powder shell pore structure. There were some connected regions around the splat interfaces and could be seen as newly formed

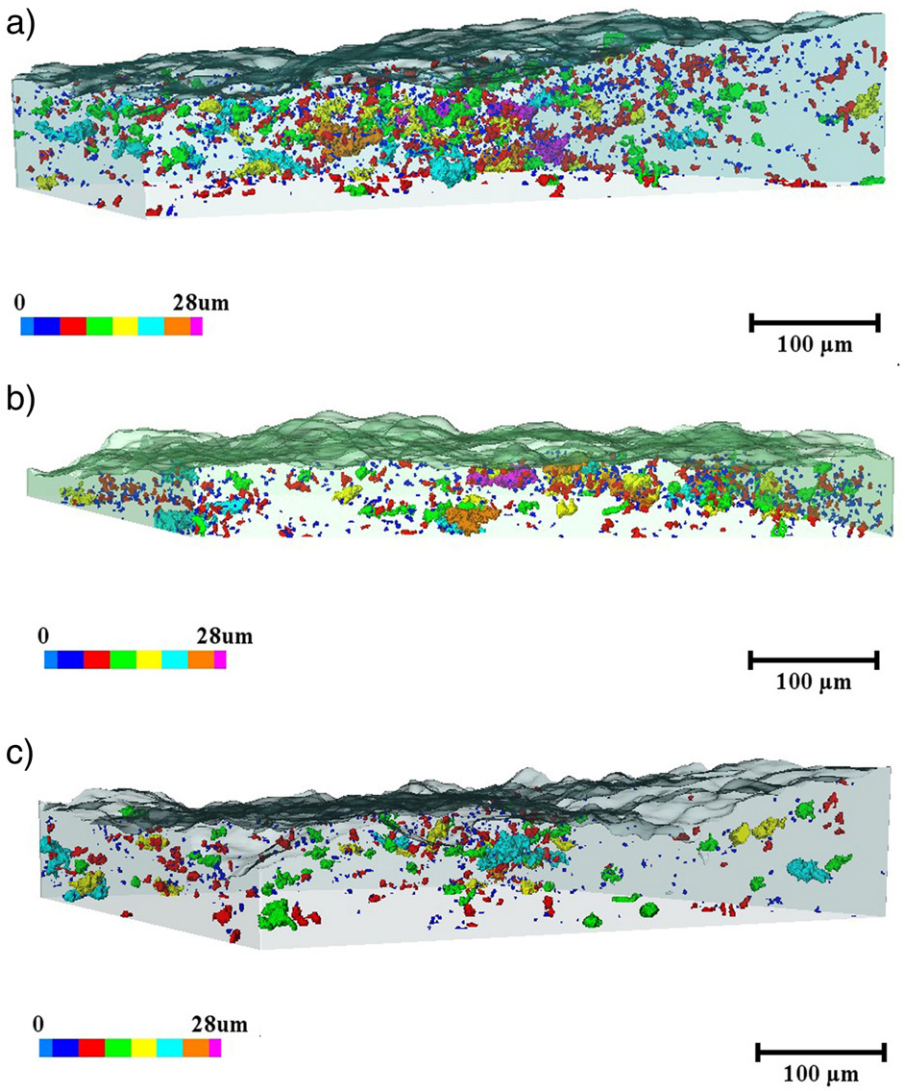

Fig. 5. 3D distribution of the pores in the coatings deposited with different powers: (a) 35 kW, (b) 40 kW and (c) 45 kW.

pores as marked by arrows B in Fig. 4. They were different with the inherited pores or newly formed broken pores. At last, there were some unconnected regions among the splat interfaces or cracks in the powders interfaces which could be seen as big open pores as marked by arrows C in Fig. 4. They could be counted statistically through XRT analysis. Therefore, the pore structure could be sketched in Fig. 9. The pores in the coatings could be classified into four types. The first one was inherited from the feedstock's HOSP structure, marked as type A. The second one was connected regions among the splat interfaces which could be seen as newly formed closed pore, marked as type B. The third one was unconnected pores or cracks, marked as type C, which existed in unconnected zones among several powders or cracks in the powder interfaces in the coatings. The last one was open pore, marked as type D, which was mainly existed among the nano YSZ particles.

The measurement of both micro-sized pores and nano-sized pores revealed that the total porosity of the coating is dominated by the micro-sized large pores. Totally, the large pore cumulative volume fraction of the coatings deposited under the arc power of 35 kW, 40 kW and 45 kW were about 15.9%, 5.9% and 4.2%, respectively. With the increase of the plasma spray arc power, the melting degree increased so that the big pores contents including both of the inherited and new formed decreased which would lead to the decrease of the total porosity. Therefore, low arc powers were more suitable to retain the HOSP structure into the coating.

4. Conclusions

The heredity and variation from hollow spherical structured YSZ powders to coatings were investigated. Hollow spherical structure was partially inherited from HOSP powder to coating. 3D structure of the pores in the coatings were characterized and counted statistically. Four types of pores in the coatings were classified, including the first type of inherited and variated from the HOSP core structure of the powder, the second one of new formed closed pore from the connected regions, the third one of unconnected pores or cracks around powders and the fourth one of inherited from the nano-sized open pore of powder shell. The porosities of the coatings were decreased with the increase in the arc power. Therefore, low arc powers were more suitable to retain the HOSP structure into the coating.

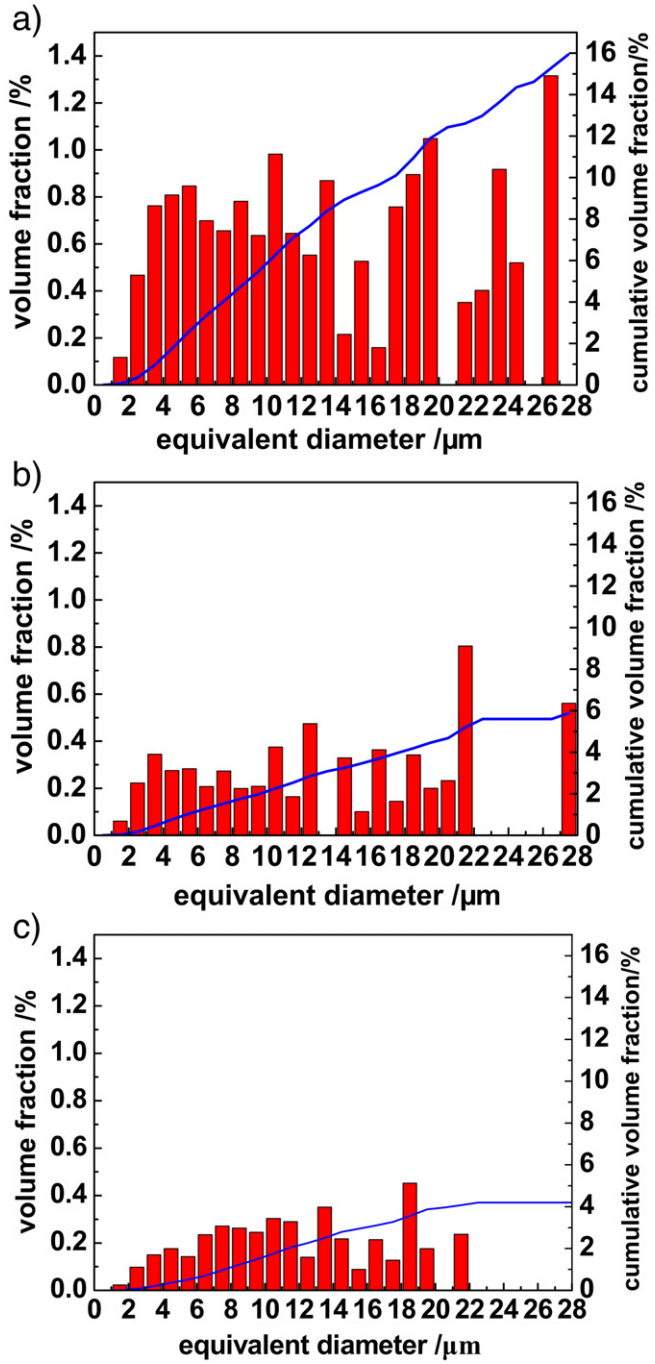

Fig. 6. Pore size and volume distribution of the coating deposited with different powers: (a) 35 kW, (b) 40 kW and (c) 45 kW.

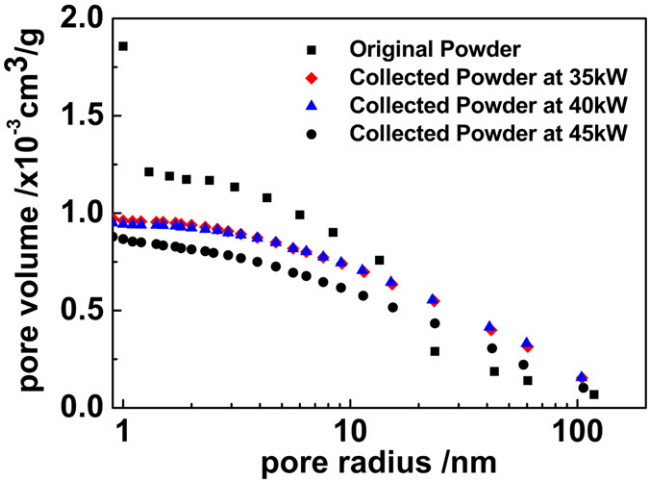

Fig. 7. Size distribution of the pores smaller than one micron in the original powder and the recollected powders after being heated within the plasma arc at 35 kW, 40 kW and 45 kW.

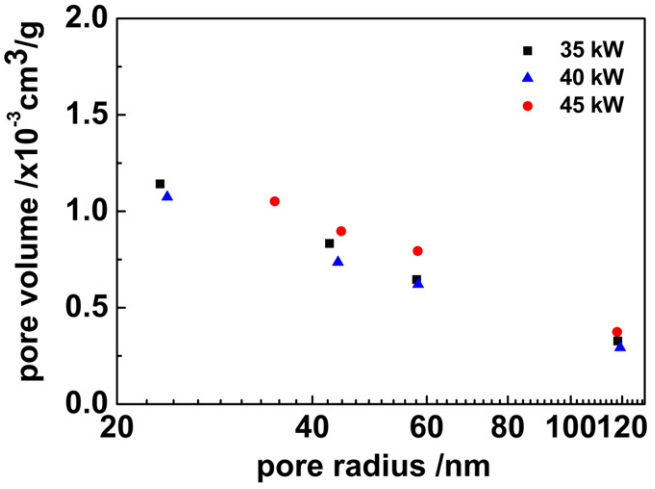

Fig. 8. Size distribution of the pores smaller than one micron in the coatings deposited at 35 kW, 40 kW and 45 kW.

Acknowledgements

This work was supported by the National Basic Research Program of China (No. 2012CB619602-3 and 2012CB619606-2), State Key Laboratory for Mechanical Behavior of Material (20131303), Special Research Program of Shaanxi Provincial Department of Education (16JK1382,16JS044), Transformation of Major Scientific and Technological Achievements in Shaanxi Province (2013KTCG01-04). The authors are grateful to Dr. Jian-Chao Pang and Shao-Gang Wang of Metal Institute, Chinese Academy of Science for advanced X-ray inspection using the VersaXRM-500 machine.

Table 2
Cumulative volume fraction and density in ceramic coatings.

Arc power/kW	Cumulative volume fraction/%	Tested density/g/cm^3
35	15.9	4.93
40	5.9	5.52
45	4.2	5.61

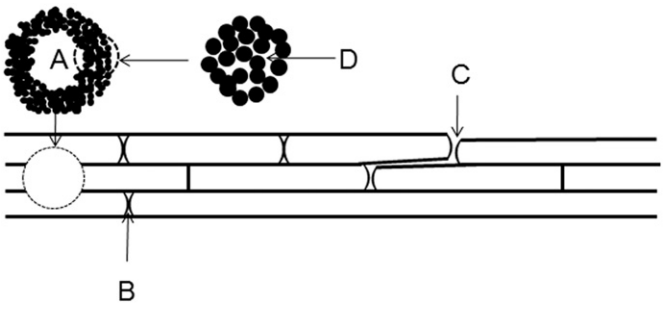

Fig. 9. Sketch of the pore structures in the coatings.

References

[1] N.P. Padture, M. Gell, E.H. Jordan, Thermal barrier coatings for gas-turbine engine applications, Science 296 (2002) 280–284.
[2] R.A. Miller, Thermal barrier coatings for aircraft engines: history and directions, J. Therm. Spray Technol. 6 (1997) 35–42.
[3] D.R. Clarke, S.R. Phillpot, Thermal barrier coating materials, Mater. Today 8 (2005) 22–29.
[4] Y. Zhao, Y. Gao, Deposition of nanostructured YSZ coating from spray-dried particles with no heat treatment, Appl. Surf. Sci. 346 (2015) 406–414.
[5] Y.S. Tian, C.Z. Chen, D.Y. Wang, Q. Ji, Recent developments in zirconia thermal barrier coatings, Surf. Rev. Lett. 12 (2005) 369–378.
[6] N. Curry, N. Markocsan, X.H. Li, A. Tricoire, M. Dorfman, Next generation thermal barrier coatings for the gas turbine industry, J. Therm. Spray Technol. 11 (2011) 108–115.
[7] R. Darolia, Thermal barrier coatings technology: critical review, progress update, remaining challenges and prospects, Int. Mater. Rev. 58 (2013) 315–348.
[8] D.R. Clarke, C.G. Levi, Materials design for the next generation thermal barrier coatings, Annu. Rev. Mater. Res. 33 (2003) 383–417.
[9] L.B. Chen, Yttria-stabilized zirconia thermal barrier coatings-a review, Surf. Rev. Lett. 13 (2006) 535–544.
[10] R. McPherson, The relation between the mechanism of formation, microstructure and properties of plasma sprayed coatings, Thin Solid Films 83 (1981) 297–310.
[11] R. McPherson, A review of microstructure and properties of plasma sprayed coatings, Surf. Coat. Technol. 39–40 (1989) 173–181.
[12] R. Taylor, J.R. Brandon, P. Morrell, Microstructure, composition and property relationships of plasma sprayed thermal barrier coatings, Surf. Coat. Technol. 50 (1992) 141–149.
[13] K. Brinkiene, R. Kezelis, Correlations between processing parameters and microstructure for YSZ films produced by plasma spray technique, J. Eur. Ceram. Soc. 24 (2004) 1095–1099.
[14] A. Kulkarni, A. Vaidya, A. Goland, S. Sampath, H. Herman, Processing effects on porosity-property correlations in plasma sprayed yttria-stabilized zirconia coatings, Mater. Sci. Eng. A 359 (2003) 100–111.
[15] Z. Wang, A. Kulkarni, S. Deshpande, T. Nakamura, H. Herman, Effects of pores and interfaces on effective properties of plasma sprayed zirconia coatings, Acta Mater. 51 (2003) 5319–5334.
[16] G. Bertrand, P. Bertrand, P. Roy, C. Rio, R. Mevrel, Low conductivity plasma sprayed thermal barrier coating using hollow psz spheres: correlation between thermo physical properties and microstructure, Surf. Coat. Technol. 202 (2008) 1994–2001.
[17] I. Sevostianov, M. Kachanov, J. Ruud, P. Lorraine, M. Dubois, Quantitative characterization of microstructures of plasma-sprayed coatings and their conductive and elastic properties, Mater. Sci. Eng. A386 (2004) 164–174.
[18] Y. Wang, Y. Bai, K. Liu, J.W. Wang, Y.X. Kang, J.R. Li, H.Y. Chen, B.Q. Li, Microstructural evolution of plasma sprayed submicron-/nano-zirconia-based thermal barrier coatings, Appl. Surf. Sci. 363 (2016) 101–112.
[19] B. Ercan, K.J. Bowman, R.W. Trice, H. Wang, W. Porter, Effect of initial powder morphology on thermal and mechanical properties of stand-alone plasma-sprayed 7 wt.% Y_2O_3-ZrO_2 coatings, Mater. Sci. Eng. A 435–436 (2006) 212–220.
[20] H.B. Guo, H. Murakami, S. Kuroda, Effect of hollow spherical powder size distribution on porosity and segmentation cracks in thermal barrier coatings, J. Am. Ceram. Soc. 89 (2006) 3797–3804.
[21] S.D. Zhang, W.L. Zhang, S.G. Wang, X.J. Gu, J.Q. Wang, Characterisation of three dimensional porosity in an Fe-based amorphous coating and its correlation with corrosion behaviour, Corros. Sci. 93 (2015) 211–221.
[22] S.S. Manickam, J. Gelb, J.R. McCutcheon, Pore structure characterization of asymmetric membranes: non-destructive characterization of porosity and tortuosity, J. Membr. Sci. 454 (2014) 549–554.
[23] A. Kumar, S. Gu, H. Tabbara, S. Kamnis, Study of impingement of hollow ZrO_2 droplets onto a substrate, Surf. Coat. Technol. 220 (2012) 164–169.
[24] R. Vaßen, F. Traeger, D. Stöver, Correlation between spraying conditions and microcrack density and their influence on thermal cycling life of thermal barrier coatings, J. Therm. Spray Technol. 13 (2004) 396–404.
[25] R.W. Trice, K.T. Faber, Role of lamellae morphology on the microstructural development and mechanical properties of small-particle plasma-sprayed alumina, J. Am. Ceram. Soc. 83 (2000) 889–896.